Chinese Journal of
POLYMER SCIENCE

RESEARCH ARTICLE

https://doi.org/10.1007/s10118-022-2734-0
Chinese J. Polym. Sci. **2022**, *40*, 1269–1286

Addition of Thermoplastic Starch (TPS) to Binary Blends of Poly(lactic acid) (PLA) with Poly(butylene adipate-*co*-terephthalate) (PBAT): Extrusion Compounding, Cast Extrusion and Thermoforming of Home Compostable Materials

Clizia Aversa and Massimiliano Barletta*

Università degli Studi Roma Tre, Dipartimento di Ingegneria Industriale, Elettronica e Meccanica, Via della Vasca Navale 79, 00146 Roma, Italy

Abstract Development of home compostable materials based on bioavailable polymers is of high strategic interest as they ensure a significant reduction of the environmental footprint in many production sectors. In this work, the addition of thermoplastic starch to binary PLA/PBAT blends was studied. The compounds were obtained by a reactive extrusion process by means of a co-rotating twin screw extruder. Thermo-mechanical, physical and chemical characterization tests were carried out to highlight the effectiveness of the material design strategy. The compounds were subsequently reprocessed by cast extrusion and thermoforming in order to obtain products suitable for the storage of hot food. The extruded films and the thermoformed containers were further characterized to highlight their thermo-mechanical, physical and chemical properties. Thermo-rheological, mechanical and physical properties of the material and of the cast film were analyzed thoroughly using combined technique as capillary rheometer, MFI, DSC, VICAT/HDT, XRD, FTIR, UV-Vis, SEM, permeability and, lastly, running preliminary chemical inertness and biodegradation tests. Particular attention was also devoted to the evaluation of the thermo-mechanical resistance of the thermoformed containers, where the PLA / PBAT /TPS blends proved to be very effective, also presenting a high disintegration rate in ambient conditions.

Keywords Thermoplastic starch (TPS); Poly(lactic acid) (PLA); Poly(butylene adipate-*co*-terephthalate) (PBAT); Extrusion; Thermoforming; Compostability

Citation: Aversa, C.; Barletta, M. Addition of thermoplastic starch (TPS) to binary blends of poly(lactic acid) (PLA) with poly(butylene adipate-*co*-terephthalate) (PBAT): extrusion compounding, cast extrusion and thermoforming of home compostable materials. *Chinese J. Polym. Sci.* **2022**, *40*, 1269–1286.

INTRODUCTION

Compostable polymers represent an extremely interesting technical-scientific alternative to conventional polymers to reduce the environmental footprint of plastics in numerous production sectors. The use of compostable polyesters is, however, still controversial, as life cycle analyzes (LCA) have not ascertained their lower environmental impact compared to polymers from fossil sources[1,2] and no-plastic materials.[3] Among bioavailable polymers thermoplastic starch (TPS) has a major strategic relevance due to its wide availability and low cost. The introduction of TPS in bioplastic products can lead to a reduction of greenhouse gas (GHG) emissions by up to 80% and the use of non-renewable energy (NREU) up to 60%.[4] TPS has inherent shortcomings that limit its widespread application in the packaging manufacturing: inadequate thermo-mechanical and chemical-physical properties. However, it is commonly modified by adding other polymeric phases, additives and reinforcing agents to obtain blends with adequate properties.[5] TPS is commonly blended with poly(butylene adipate-*co*-terephthalate) (PBAT) for the manufacturing of flexible films by blown extrusion.[6–12] The most common studies include the use of compatibilizers based on maleate species,[6,10] and organic acids.[7,12] Further studies evaluate the influence of the composition of the blend (*i.e.*, the ratio between TPS and PBAT, type of plasticizer, addition of process additives) and of the process parameters (*i.e.*, thermal profile, flow rate, shear stress) on performance of semi-finished products (compounds) and films.[8,9,11] Efforts to improve TPS-based blends have been carried out for over 20 years,[13] however, applicability of such blends is essentially limited to the segment of flexible thin films produced by blown extrusion (thickness 10–100 μm).[14,5] Applications in rigid and semi-rigid packaging manufacturing are extremely rare.[15–17] Therefore, cast extrusion of high thickness films (range 100–1000 μm) containing TPS is still largely unexplored as well as the thermoforming process of high thickness films into relatively complex shaped products.[18,19] This kind of items is widely used as rigid and

* Corresponding author, E-mail: massimiliano.barletta@uniroma3.it
Received January 28, 2022; Accepted March 12, 2022; Published online May 31, 2022

© Chinese Chemical Society
Institute of Chemistry, Chinese Academy of Sciences

semi-rigid packaging for the storage of numerous fresh food products such as meat, cheese, pasta, allowing their correct preservation and shelf life increase.[20] However, this type of packaging requires the use of plastic materials that combine formability with several technological properties such as thermo-mechanical resistance, impermeability to gases (oxygen, water vapor, carbon dioxide, *etc.*) and liquids, protection from photo-oxidation, suitability for prolonged food contact, compostability despite high thickness,[21–23] preferably in ambient conditions. At the present stage, the proposed packaging solutions in the literature and by technicians and practitioners are mostly based on the intrinsically thermally resistant PBS, which is, however, extremely expensive, and often made entirely from fossil resource. Here, a compound that are fast to degrade (possibly, even in domestic facilities) and involve the bioavailable starch and bioderived PLA is proposed, with the final purpose to reduce the related environmental impact. Specifically, the present work aims to study the addition of TPS (25 wt%) inside PLA/PBAT (partially bio-derived) blends for the manufacturing of compounds suitable for cast extrusion and thermoforming of semi-rigid containers for the packaging of foodstuffs. Particular attention has been paid to the thermo-mechanical resistance of the products, demonstrating the good performance of the PLA/PBAT blend even after the addition of a high TPS content, together with a high disintegration rate in ambient conditions.

EXPERIMENTAL

Materials

PBAT, an aliphatic-aromatic polyester from fossil and compostable sources, was purchased from BASF SE Biodegradable Polymers (Ludwigshafen, Germany). The PBAT grade chosen for this study is characterized by a molecular weight M_w of 1.76×10^5 g/mol and a polydispersion index PDI of 1.75.[24]

PLA, an aliphatic polyester 100% bio-derived and compostable up to 2.3 mm thick according to the EN13432 standard, was purchased from Total Corbion PLA bv (Gorinchem, The Netherlands). The selected grade is Luminy L175. Luminy® L175 is a high heat, high viscosity, PLA homopolymer (>99% L-isomer, molecular weight M_w 2.26×10^5 g/mol, polydispersity index PDI 2.184.[25] Compared to standard PLA, these PLA homopolymers have higher melting points and an increased rate of crystallization. As a result, compounds containing PLA homopolymers are suitable for the production of semicrystalline parts, which exhibit a higher temperature resistance.

The main properties of the PLA and PBAT grades chosen for this study are summarized in Table 1.

TPS was purchased from Agrana Starke Gmbh (Gmund, Austria). In particular, Amitroplast 8945 is a TPS with a 100% bio-derived carbon content, compostable at room temperature. Suitably dispersed within the PBAT, Amitroplast 8945 can ensure the production of flexible films with elongation percentages up to 350% and tensile strength of about 25 MPa (or up to 60 MPa for oriented films).

The talc was supplied by Imerys Talc (Paris, France). A high performance lamellar micronized talc (Luzenac HAR W92) was selected. Dispersed within the plastic materials, it increases the elastic modulus, thermal resistance and impact resistance. Finally, ethylene bis (stearamide) (EBS), an amide wax with a slip and anti-block function, was purchased by Croda Italiana Spa (Mortara (PV), Italy). In particular, Crodamide EBSV, an amide wax of entirely vegetable origin, was chosen.

Processing

The formulation studied is reported in Table 2, it is a ternary blend based on PBAT, TPS and PLA (short named B-TPS1). The formulation has a TPS content of 25 wt%, which was added to increase compostability and reduce the overall cost of raw materials of the blend. PLA was introduced in a 4:9 weight ratio (about 30 wt%) with the other polyester (PBAT). Talc was added at 8 wt% to simplify the cutting operation of the pellets. EBSV was added at 2 wt% to favor homogeneous dispersion and distribution of the various constituents of the blend. Amide waxes are also used to avoid sticking of the material on the rollers during the film preparation phase by cast extrusion and ease the extraction of the product from the mold at the end of the thermoforming processes. Moreover, B-TPS1 formulation is designed to be biodegradable, in accordance with ISO 14855.

The compounds were extruded with a twin-screw co-rotating extruder using a 27 mm, *L*/*D* (Length to Diameter) = 40 apparatus (ZSE 27 IMaxx, Leistritz Extrusionstechnik Gmbh, Nurnberg, Germany). After processing, the compounds were dried in a dehumidifier (DW250I-MT, Plastic System Srl, Borgoricco (PD), Italy) at 50 °C for 3.5 h. The compounds were obtained by setting the process parameters shown in Table 3. Dehumidified compounds were then reprocessed by cast extrusion using a lab-scale device (Minicast 20, Eurexma Srl, Venegano Superiore (VA), Italy). The system is based on a 20 mm of diameter single-screw extruder equipped with a volumetric feeding hopper for pellets. The extruder has a ratio *L*/*D*=30/1. The vertical axis die is 200 mm wide an is equipped with adjustment pins for the manual regulation of the thickness of the extruded film between 100 and 1000 μm. The die is characterized by three individual thermal control zones (left, central, right). The system is setup with two chromed steel rollers with a diameter of 300 mm, water cooled and characterized by adjustable rotation speed. Lastly, the system is equipped with a motorized towing device with adjustable

Table 1 Typical properties of the materials.

Materials	MFI ISO 1133-A (190 °C/2.16kg)	Melting point (°C) DSC	Tensile Modulus (MPa) ISO 527-1	Tensile strength (MPa) ISO 527-1	Elongation at break ISO 527-1	HDT (°C) (amorphous) ISO 75-1	Charpy (23 °C) ISO 179
PLA Luminy L175	3 g/10min	175	3500	50	<5%	60	<5 kJ/m^2
PBAT Ecoflex C1200	3.8 g/10min	110–120	105–132	35–44	560%-710%	35–46	na

https://doi.org/10.1007/s10118-022-2734-0

Table 2 Details of the investigated formulations.

Materials	B-TPS1 (wt%)
Amitroplast 8945	25
PLA (Luminy L175)	20
PBAT (Ecoflex C1200)	45
Luzenac HARW92	8
Crodamide EBSV	2
Total	100

speed for winding the film on the reel. In this study, films with ~500 μm thickness and ~200 mm width were obtained by setting the process parameters shown in Table 4. The thermoforming process was carried out using a pilot device equipped with a single cavity mold (450 DT, Formech International Limited, Thrales End, United Kingdom). The device is characterized by four heating zones (upper, lower, lateral and central) with individual control, heated by quartz lamps. The thermoforming operation takes place by applying vacuum inside the mold, ensuring a maximum working area of 430 mm × 280 mm. The product obtained is shown in Fig. 1. The heating time was set to 30 s. The heating powers of the lateral, upper and lower zones were set at 70%, while the heating power of the central area has been set at 80%.

Characterization

The melt flow index (MFI) of the compounds was measured according to the reference standard ISO 1133-1:2011(E) using the test method A (weight/MFI), through the MFI-1221 XNR-400B apparatus (Amse, Settimo Torinese (TO), Italy), equipped with an automatic extrudate cutting device. Specifically, the MFI was evaluated on the compounds at 210 and 230 °C, applying a weight of 2.16 kg.

Apparent viscosity of the compounds was measured at 180 °C varying the shear rate in the range of 50 s^{-1} to 2000 s^{-1}, at thirteen different shear rates: 50, 100, 250, 350, 500, 650, 750, 850, 1000, 1250, 1500, 2000 s^{-1}. The tests were performed using a CEAST SR20 (Norwood, Massachusetts, United States), advanced bench-top capillary rheometer, piston-die type, according to ISO 11443 reference standard. The capillary rheometer is characterized by a length-to-inner diameter ratio (*L*/*D*) of the die of 20 mm/mm and is setup with a 20 mm of length and 1 mm of diameter capillary and a 15 mm of diameter barrel. The flow rate is applied by a piston and the melt pressure is measured by a transducer. 30 g of material were weighted and manually packed. A compacting force of 300 N was then applied during 5 min preheat cycle to ensure a homogenous packing and uniform heating of the sample.

HDT (heat deflection temperature) tests were performed according to ISO 75-B reference standard using the apparatus HDT/V-1113 (Amse, Settimo Torinese (TO), Italy). Test parameters are: pressure set to 0.45 MPa and heating rate set to 120 °C/h. The standard specimens were prepared using a TMSP2 bench injection press (Amse, Settimo Torinese (TO), Italy), setting a hot chamber temperature of 190 °C, a mold temperature of 50 °C, a time of maintenance of 4 min and an injection pressure of 4.5 bar.

Vicat tests were carried out on the same apparatus and with similar methods, according to ISO 306 standard, B/50N method. In this case, the load applied to the specimens was 50 N with a heating rate of 50 ° C/h.

Thermal analysis was performed using a differential scanning calorimeter (DSC) DSC3 (Mettler Toledo, Columbus, Ohio, United States). The samples underwent three scans: first heating scan, second cooling scan and third heating scan. B-TPS1 formulation (~5–7 mg in pellet form, film sample and thermoformed sample) was analyzed in the range of 30–250 °C with a heating/cooling rate of 10 °C/min. Measurements of the main thermodynamic properties were registered from the first scan, as this can provide information on the thermal history (previous processing) of the material. The analyzed properties are: (i) T_g glass transition temperature of the semi-crystalline polymers in the blend; (ii) T_{cc} cold crystallization temperature; (iii) T_c crystallization temperature; (iv) T_{hc} solid phase secondary transition temperature; (v) T_m melting temperature of each semi-crystalline polymer in the blend; (vi) X_c crystalline fraction of each polymeric component.

The crystallinity value X_c is calculated using the following equation (Eq. 1):

$$X_{c,i}\,(\%) = \frac{\Delta H_m - \Delta H_{cc}}{\Delta H_m^{\circ} \times \Phi_i} \quad (1)$$

where $X_{c,i}$ (%) is the weigth percentage of crystalline fraction referred to the content of the i-polymeric phase, ΔH_m° is the standard molar melting enthalpy referred to a hypothetical 100% crystalline sample, ΔH_m and ΔH_{cc} are, respectively, the molar enthalpy and the cold crystallization enthalpy experimentally detected on the sample under examination, Φ_i is the weight fraction of the polymer under examination with

Table 3 Processing parameters for the manufacturing of the compounds B-TPS1.

Screw speed (r/min):	600			Melt temperature (°C):						164
Screw speed (side-feeder) (r/min):	256			Melt pressure (bar):						24
Blade cutting speed (water ring) (%):	60			Torque (%):						38
Set throughput (kg/h):	42			Measured throughput (kg/h):						40.8
Thermal profile (°C)	*T*1	*T*2	*T*3	*T*4	*T*5	*T*6	*T*7	*T*8	*T*9	Head
	175	180	178	170	165	160	155	150	145	162

Table 4 Processing parameters for the cast extrusion of the compounds B-TPS1.

ID	Thermal profile (°C)							Screw speed, v_e (r/min)	Roll speed, v_c (m/min)	Haul-off speed, v_t (m/min)	Reel speed, v_a (%)	Thickness (μm)	Width (mm)
	*T*1	*T*2	*T*3	*T*4	Head								
					T_{left}	T_{middle}	T_{right}						
B-TPS1	175	180	185	185	185	185	185	133	1	1.3	28	505±5	202

https://doi.org/10.1007/s10118-022-2734-0

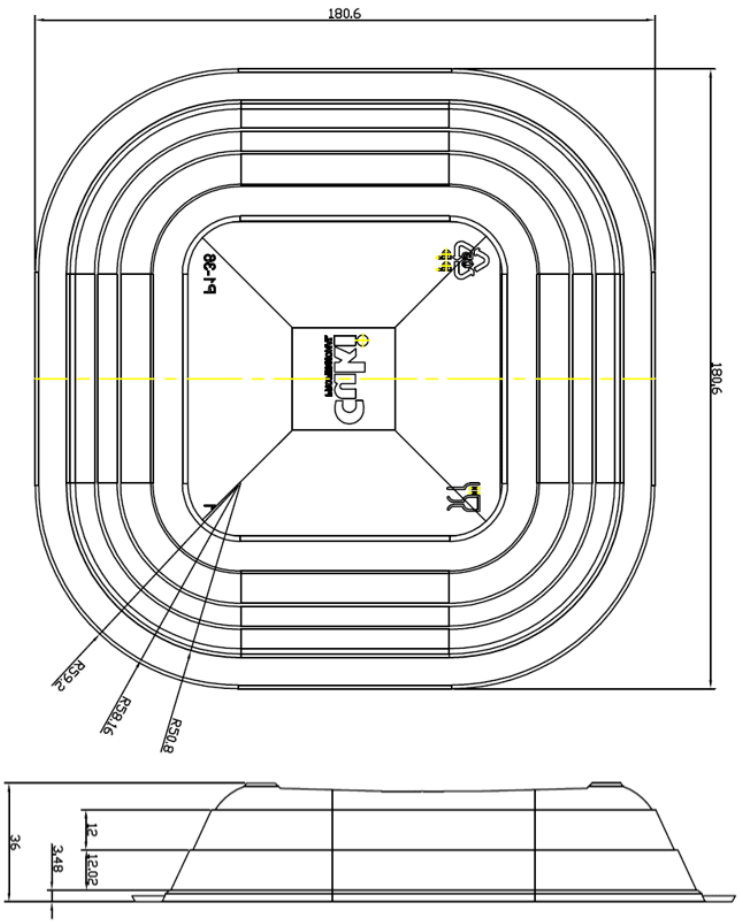

Fig. 1 Design of the thermoformed items.

respect to the total weight of the blend. The experimental ΔH_m value is calculated as the area underlying the endothermic melting peaks, subtracting the area underlying the exothermic crystallization peaks.

XRD tests were performed on compounds, films and thermoformed samples at ambient conditions by means of an XRD apparatus (Smartlab SE, Rigaku Coorporation, Tokyo, Japan) with Cu-Kα radiation source (λ=1.54 Å) at voltage 40 kV and current 40 mA. Intensities were collected by step scanning in the 10°–80° (2θ) range, with a step of 0.01° and a counting time of 1 s for each step.

FTIR (Fourier-transform infrared spectroscopy) analyzes were carried out in ATR (Attenuated Total Reflection) mode with a Jasco 6600 instrument (Jasco Inc., Easton, Maryland, United States) equipped with an ATR optical system (PRO ONE, Jasco Inc., Easton, Maryland, United States). The spectra were recorded in transmittance, obtaining the final spectrum through the automatic processing of the average on 30 spectra, acquired for each sample, with a resolution of 2 cm^{-1} in the range between 4000 and 600 cm^{-1}. Spectra were treated with baseline subtraction, normalization and expressed in absorbance. The tests were carried out on pellet and film samples. Since no significant variation was observed between pellets and film samples, the test was not carried out on thermoformed samples.

The cross section of the specimens was observed using the secondary electron (SE) mode of a Coxem CX200Plus scanning electron microscope (Yuseong-gu, Daejeon, South Korea). The system is equipped with a variable acceleration voltage between 1 and 30 kV. It can operate in both compositional and topographic secondary electron (SE) or back scatter (BS) modes. Before observation, the specimens were sputtered with a thin layer of gold by means of a sputter coater (108 auto, Cressington), setting current intensity to 20 mA and deposition time to 30 s in vacuum (0.001 mbar). The magnification selected in the observations is 1000×. The acceleration voltage of the electrons was set at 18 kV.

The films obtained by cast extrusion with a thickness of about 500 μm were characterized by a static tensile test, performed in accordance with the ASTM D638-14 standard, specific for thin films (thickness <4 mm). The test was performed using an LR 5K dynamometer (Lloyd Instruments, Bognor Regis, United Kingdom) equipped with a 2000 N load cell, applying a crosshead speed of 50 mm/min. The tests were performed on five replicates for each direction of the sample: five in the direction of the extrusion process (machining direction, MD) and five in the direction perpendicular to the extrusion process (Transversal direction, TD). The specimens were die-cut according to the standard geometry (ASTM D638-14). The following properties were obtained from the test: elastic modulus (E_y, MPa), yealding stress σ_y (MPa), stress at break (σ_b, MPa), maximum strain ε_b (%).

https://doi.org/10.1007/s10118-022-2734-0

Oxygen permeability tests were performed on film samples by means of permeabilimeter TotalPerm (Extra Solution PermTech, Pieve Fosciana (LU), Italy). The selected instrument is able to measure the permeability even on gases other than oxygen, in particular water vapor and carbon dioxide, by operating on flat samples or on samples of complex shape through the use of a special adapter. The central part of the instrument is constituted by the measuring cell, which, once the flat sample has been assembled, remains divided into two "half-cells". The gas being analyzed (oxygen) is flowed in a controlled manner inside the upper half-cell, while the carrier gas (nitrogen) is flowed into the second half-cell. The gas pressure in the two half-cells is kept constant at 1 atm, so that any possible passage of gas being analyzed towards the half-cell with carrier gas can be attributed exclusively to the permeability of the membrane (thermodynamic equilibrium). The measurement is divided into two successive phases: conditioning and testing. During the conditioning phase, the carrier gas is flowed inside both half-cells. This flushing has the purpose of removing any residual oxygen, water and carbon dioxide from samples and semi-cells, so as not to have an overestimation of the results during the actual measurement. The removal of these residual elements also involves the bulk part (the thickness) of the film under examination and will have a shorter duration (easy removal) the more the material will be breathable. Once the plateau has been reached (zero value of the contaminating gases), the test is started by flushing the permeating gas, specifically pure oxygen, into the upper chamber. The coloumbometric sensor, connected with the gas flow coming from the lower chamber, will detect the passage of oxygen through the film, which will proceed from the upper chamber to the lower one the faster the more breathable the film under examination. The system is structured to control the temperature and humidity of the two half-cells, so that these two parameters remain constant during the measurement. The measurement was performed setting the carrier gas flow rate as 11.78 cm^3/min, relative humidity as 50% and temperature as 23 °C.

Light radiation transmission test of the extruded films in the UV-Vis spectrum was carried out with a UV-Vis-NIR V-670 spectrophotometer operating in the UV-C/near IR range (Jasco Inc., Easton, Maryland, United States), equipped with a D2/WI light source and an ISN-723 single beam integrating sphere (Jasco Inc., Easton, Maryland, United States) capable of operating on solid samples. The measurements were performed using a monochromatic ray characterized by a spectral band of 5 nm, applying a scanning speed of 1000 nm/min in the wavelength range of 190–800 nm and setting a 0.5 nm step.

Chemical resistance tests were carried out on extruded films, immersing the samples in different solutions (NaCl, 3 wt% solution, vinegar, ethanol, seed oil, 1 wt% NaOH solution, 1 wt% HCl solution) and recording morphological and surface variations at defined time intervals by means of a digital camera. The measurement conditions (constant temperature, volume of the contaminant, *etc*.) were chosen according to UNI EN ISO 175 standard.

Thermal resistance tests were performed on the thermoformed product (plate), filling it with a 400 mL of water volume, at 65 and 100 ° C. The test was repeated in triplicate, for each temperature, using a new sample each time. The tests involved instant contact of the hot liquid with the sample. A progressive heating (like the one that occurs in microwave tests) would not be able to stress the polyesters, as these materials are able to recrystallize by thermal annealing. Conversely, they are generally not able to effectively counteract the thermal shock that is generated by direct and immediate contact with large quantities of hot liquid.

Lastly, the thermoformed plates were subjected to a compression test at ambient conditions (T=23°C, RH=50%) to evaluate the mechanical properties of the products. An internal testing method was developed starting from ASTM D695 standard, for compression tests on plastic materials, but considering a different geometry of the test samples, in this case an axisymmetric geometry (Fig. 1).

Compression tests were performed using LR 5K dynamometer (Lloyd Instruments, Bognor Regis, United Kingdom) equipped with a 2000 N load cell, set up with large compression plates. Testing parameters are: crosshead speeds set as 10, 50 and 100 mm/min, approach speed set as 2.5 mm/min, preload set as 2 N. The letters A, B, C, D in Fig. 2 show the response of the thermoformed plate to the compression load. The deformation trend of the sample during the test is related to: (i) hunching of the bottom of the plate (first rib, point A); (ii) appearance of a series of local maximum points for the load curve, where each maximum corresponds to the failure of a reinforcing element (second rib point B and third rib point C); (iii) progressive packing of the upper sections on the lower ones (point D). The tests are performed by compressing 85% of the total height of the plate. To estimate the response of the sample to the compression test, the following parameters were evaluated: (i) angular coefficient m (N/mm) of the linear section (A), rigidity of the product; (ii) value of the load C_{max} (N) before failure of the plate at point C; (iii) deformation (mm) in correspondence of load C_{max} (N); (iv) limit load at point D (N) and corresponding deformation (mm); (v) springback (mm); (vi) deformation energy (J).

Compostability Test

The compostability test in ambient conditions[26] involved the use of a composter filled with soil, wood sawdust (about 4%), water and biodegradable urban waste (about 44%). Moreover, 200 mL of pineapple juice were added to the compost to increase its acidic character. The container used to place the compost (*i.e.*, composter) was perforated in order to ensure ambient conditions during the test. Specimens of equal weight were obtained from extruded films, which were inserted inside the composter. The morphological conditions of the analyzed samples were monitored and photographed on a weekly basis. Furthermore, the weight loss was recorded, again on a weekly basis, (for a period of approximately 2 months, or 9 weeks) using an analytical scale AS220.R2 (Bioclass, Pistoia (PT), Italy), with sensitivity of 0.1 mg.

RESULTS AND DISCUSSION

Processability and Rheological Characterization

B-TPS1 formulation is characterized by the presence of TPS, PLA (bio-derivation) and PBAT (fossil source). As known in literature,[14,27,28] the presence of TPS in the formulation hinders

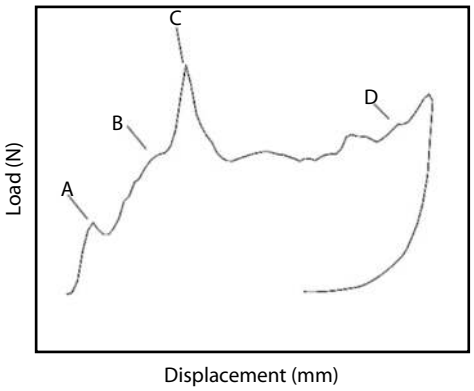

Fig. 2 Typical load-displacement trend of the compression test performed on thermoformed item.

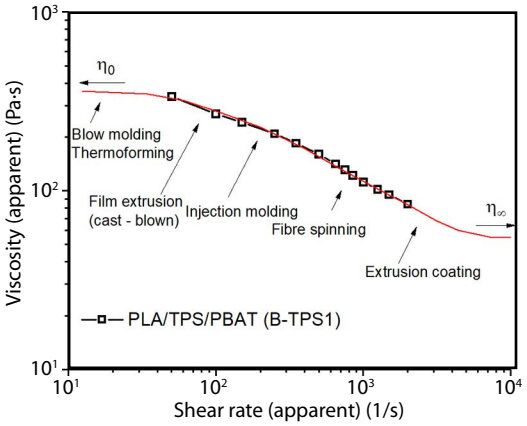

Fig. 3 Apparent viscosity versus shear rate for B-TPS1 (PLA/TPS/PBAT).

good processability of the polymer blend. TPS is a highly hydrophilic material, substantially incompatible with biodegradable polyesters which have a predominantly hydrophobic character. The partial incompatibility of TPS in binary and ternary blends with biodegradable polyesters is widely discussed by.[29] In this specific case, a high rotation speed of the screws and a screw profile characterized by very aggressive mixing elements were used to obtain a homogeneous compound. Imparting a high shear stress to the polymer melt during the extrusion process and promoting, thanks to the action of the aforementioned mixing elements, an energetic dispersive action on TPS, allows to obtain a good homogeneity of the pellets. The rheological behavior of the compound was initially examined through the evaluation of the MFI in accordance with ISO 1133-1: 2011 (E). B-TPS1 exhibits an MFI of 35.5 g/10min at 230 °C under a load of 2.16 kg. At 210 °C, the MFI value was not measurable (the material did not flow, as it was too viscous at that temperature), as expected for a material designed for cast extrusion and thermoforming processes. Fig. 3 shows the apparent viscosity trend as a function of the shear rate, evaluated by means of a capillary rheometer at 180 °C, that is, a temperature close to the temperature profile set during compounding. Formulation B-TPS1 shows a non-Newtonian behavior shear thinning type, since the viscosity decreases as the shear rate increases.

The linear section of the curves represents the shear thinning regime and can be expressed according to Eq. (2) (*i.e.*, Ostwald and de Waele power-law):

$$\tau = \mathrm{K}(T)\left(\frac{\mathrm{d}\gamma}{\mathrm{d}t}\right)^n = \mathrm{K}(T)\,\dot{\gamma}^n \qquad (2)$$

where τ is the shear stress, γ is the shear strain, $\dot{\gamma}$ is the shear rate, T is the temperature, t is the time, and K and n are empiric parameters. The apparent viscosity which is defined as the ratio $\eta = \tau/\dot{\gamma}$ can be thus expressed as Eq. (3) according to which η is described by a second order power-law equation:

$$\eta = \mathrm{K}(T)\,\dot{\gamma}^{(n-1)} \qquad (3)$$

It is possible to estimate η_0 and η_∞ for shear rates $\dot{\gamma}$=0 and $\dot{\gamma}$=∞, respectively, from the red curve showed in Fig. 3. Values extrapolated from the logarithm of viscosity are ~400 and ~50 Pa·s.

HDT/Vicat

Results of the HDT/VICAT tests performed on formulation B-TPS1 are summarized in Table 5. PBAT has a melting temperature of about 110–120 °C. It is also characterized by a VST of about 89 ° C,[30] a similar value was found for B-TPS1. Compound B-TPS1 shows a rather low HDT value (~53 °C). After all, the HDT of PBAT, which is the main phase of B-TPS1, is about 46 °C.[31]

Table 5 HDT and VICAT evaluated on B-TPS1 compounds.

Sample	VICAT (°C)	HDT (°C)
B-TPS1	87.8±5.1	53.4±1.2

Thermal Analysis

Fig. 4 summarizes the results of the thermal analysis of B-TPS1 pellets, films and thermoformed samples after extrusion compounding, cast extrusion and thermoforming processes, respectively. Table 6 summarizes the primary and secondary thermal transitions evaluated on B-TPS1.

B-TPS1 pellets (Fig. 4) show a very clear glass transition at about 57.3 °C (T_g) attributable to PLA, visible from the first scan. These pellets show an equally clear cold crystallization peak attributable to PLA at 89.3 °C (T_{cc}). PLA is known to form

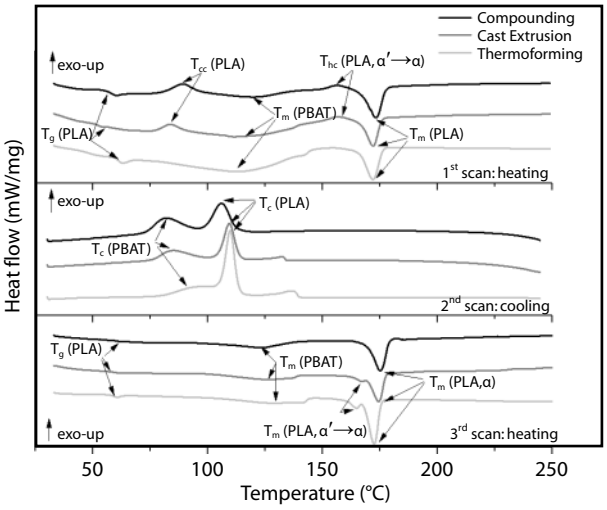

Fig. 4 Thermal analysis of compound, film and thermoformed items produced by B-TPS1.

https://doi.org/10.1007/s10118-022-2734-0

Table 6 DSC analytic data (extracted from the 1st heating and 2nd cooling scan).

Sample	T_g (°C)	T_{m1} (°C)	T_{m2} (°C)	T_{m3} (°C)	T_{cc} (°C)	T_{hc} (°C)	T_{c1} (°C)	T_{c2} (°C)	T_{c3} (°C)	X_1*	X_2*	X_3*
B-TPS1(compound)	57.3 (PLA)	119.9 (PBAT)	n.d.	173.7 (PLA)	89.3 (PLA)	156.5 (PLA)	82.5 (PBAT)	n.d.	105.7 (PLA)	5.5 (PBAT)	n.d.	27.5 (PLA)
B-TPS1(cast film)	n.d.	112.8	n.d.	172.0	83.8	n.d.	85.2	n.d.	109.2	4.6	n.d.	39.2
B-TPS1(thermoformed)	60.7	112.8	n.d.	171.8	n.d.	156.8	n.d.	n.d.	110.0	7.1	Missing	38.7

* X_1, X_2 and X_3 are the degree of crystallinity of the first, secondary and tertiary polymeric phase of B-TPS1, respectively.

α-type crystals at temperatures above 120 °C by solution crystallization, by polymer melt cooling or by cold crystallization. The α′ type crystals always develop by cooling from a polymer melt or by cold crystallization at temperatures below 100 °C. At temperatures between 100 and 120 °C, PLA crystallizes generating both α and α′ crystals.[32] Therefore, B-TPS1 pellets showing a T_{cc} <100 °C, certainly generate α′-type crystals. This result is confirmed by the large exothermic peak obtained in the first scan at ~156.5 °C (T_{hc}) which precedes the endothermic melting peak at ~173.7 °C ($T_{m,PLA}$). The exothermic peak at ~156.5 °C (T_{hc}) is indeed attributable to the solid phase transition of the α′ (disordered) phase into α (ordered) phase.[33] The first scan of B-TPS 1 pellets also shows a large melting peak of PBAT at ~120 °C ($T_{m,PBAT}$). The crystallization temperatures (T_c) of PLA and PBAT obtained in the second cooling ($T_{c,PLA}$=105.7 °C; $T_{c,PBAT}$=82.5 °C) are lower than melting temperatures ($T_{m,PLA}$=173.7 °C; $T_{m,PBAT}$=120 °C) obtained in the first heating scan due to thermal inertia phenomena.

Nonetheless, the first scans of the extruded film and of the thermoformed item obtained using the B-TPS1 pellet, show a less clear glass transition temperature. Moreover, in the case of the thermoformed sample the T_{cc} is not visible, while in the extruded film it is confirmed below 100 °C (*i.e.*, 83.8 °C). An increase in the crystallinity of PLA in the film and, above all, in the thermoformed item, is observed in accordance with.[34] The cooling trends show that the crystallization temperatures (T_c) of PLA and PBAT assume higher values for the thermoformed product ($T_{c,PLA}$=110.0 °C) compared to the extruded film ($T_{c,PLA}$=109.2 °C, $T_{c,PBAT}$=85.2 °C) and even more compared to pellets ($T_{c,PLA}$=105.7 °C, $T_{c,PBAT}$=82.5 °C). Furthermore, the crystallization peak of PLA is much sharper and wider in the case of the thermoformed item, slightly less in the film, compared to the trends observed for the pellet. The experimental evidence demonstrates the greater crystallinity of the material after cast extrusion and, even more, after the thermoforming processes.[34] The second heating scan confirms the previous experimental observations. In this case, the glass transition temperature is almost undetectable for the pellet, the extruded film and the thermoformed product. Similarly, it is not possible to observe the presence of peaks attributable to cold crystallization. Only melting peaks of PBAT and PLA are clearly visible, thus confirming the hypothesis that repeated heating and cooling cycles (which is what occurs for cast extrusion and thermoforming) favor the crystallization of the material. The observation of the melting peak of PLA reveals a reduction in the melting temperature in the case of the film sample ($T_{m,PLA}$=174.6 °C) and, above all, of the thermoformed sample ($T_{m,PLA}$=172.3 °C) with respect to the pellet ($T_{m,PLA}$=175.1 °C). Furthermore, in the film and in the thermoformed samples an endothermic peak is visible at temperature below the main melting peak, which is ascribable to the transformation of the α' (disordered) phase into the α (ordered) phase. However, in this case, the transformation phenomenon occurs through the recrystallization mechanism during melting according to what was previously observed in Ref. [33].

XRD Analysis

Fig. 5 shows the XRD patterns for 2θ values between 10° and 35° in the case of the compound, the film and the thermoformed sample. This range allows to emphasize the peaks of the polymeric phases used in the formulation, which are mainly concentrated at low angles, not considering most of the peaks associated to talc (inert material) which are instead present in the range of 2θ between 10° and 80°, as they are not considered relevant for the topics covered in this work. The signal is less clear for compounds due to the irregular surface of the examined sample (*i.e.*, extremely corrugated morphology of the pellets). On the other hand extruded films and thermoformed products are characterized by a more regular and homogeneous morphology therefore a cleaner spectrum was detected. Fig. 5 shows the reflections of the typical crystalline structure of PBAT with peaks in the 2θ region between 15° and 30° in agreement with Ref. [35].

In particular, the following five peaks were identified: 16.6° (α-PBAT, 011), 17.4° (α-PBAT, 010), 20.0° (α-PBAT, 110), 23.8° (α-PBAT, 100) and 25.7° (α-PBAT, 111) in accordance with results reported in literature.[36] It is assumed that PBAT crystallizes in a triclinic α configuration (α-form triclinic). There are shifts in the peaks compared to what is reported in the literature.[35] However, the shifts can be attributed to the irregular geometry of the pellets which affects the signal acquisition during the XRD test. The shifts are very common when examining the data in the literature. Furthermore, the modest intensity of the diffraction peaks and the large shape of the reflections denotes a modest crystallization of PBAT, according to the results of the thermograms. From the examination of Fig. 6 it is also possible to highlight the presence of some peaks attributable to TPS. Starch exhibits different peaks whether it is in native or plasticized form.[37] The native starch exhibits three crystalline structures, respectively called A-, B- and C-type, double-helical type, in a monoclinic configuration. However, the plasticization starch that occurs in a compounding process determines the destruction of the crystalline configuration of the native starch and the generation of an amorphous material which, subsequently, tends to recrystallize.

Basically, during the starch compounding process in the presence of plasticizer, the typical hydrogen bonds of native starch are replaced by the formation of bonds between the starch and the plasticizer itself. The formation of such bonds is favored by high temperatures and significant shear forces [38]. The recrystallization that takes place during the formation of TPS determines the mutation of the crystalline structure from a double helix to a single helix one (single helical).

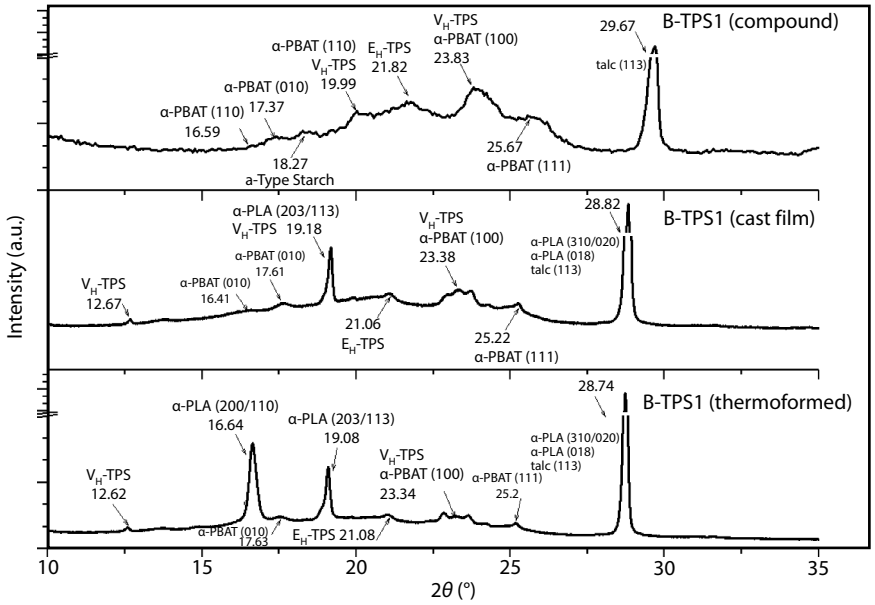

Fig. 5 XRD patterns of compound, film and thermoformed items produced by B-TPS1.

These structures are commonly classified as VH-, VA- and EH-characterized by a hexagonal configuration, which differ in the packing level of the helix and in the hydration level (the subscript H is associated with hydrated forms, the subscript A it is instead associated with anhydrous forms). In this case, there are no peak attributable to native starch, confirming the dismantling of native starch at the end of the extrusion process. The peaks present at 20.0° and 23.8° can presumably be ascribed to the crystalline form VH-TPS, whereas the peak at 21.8° can, on the other hand, be ascribed to the EH-TPS form. However, the crystalline structure of TPS is also dependent on humidity, so the signals of the XRD test could also be influenced by environmental conditions.[37] Finally, the peak at 29.7° can be attributed to the reflection plane (113) of talc. Slight shifts of talc peaks are caused by higher values of 2θ due to the thermo-compression and shear stresses to which the talc particles are subjected during the compound extrusion process.[38] There is apparently no peak attributable to PLA in compound B-TPS1, presumably because the cristallinity degree is very low. Lastly, it is possible to observe the wide amorphous band included in the 2θ region between 17° and 27°, attributable to non-crystallized polymeric phases inside the compound.

The spectra of B-TPS1after cast extrusion and thermoforming process show the presence of crystalline peaks attributable to PLA. The reprocessing of the B-TPS1 compound by cast extrusion and thermoforming favors the crystallization of PLA in accordance with what is observed in the DSC thermograms. In particular, following the cast extrusion process, reflections (203/113) of the α crystalline phase of PLA into an orthorhombic configuration are visible according to the peak located at 2θ=19.2°. A second peak at 28.8° is visible (partially superimposed on the talc peak), which is associated with reflections (310, 020, 018).[39] The spectrum of the film obtained by cast extrusion shows a peak at 2θ=12.7° attributable to TPS (VH-TPS), shifts in the peaks associated to PBAT and talc which are attributable to the reprocessing of the material (the re-grinding of talc determines the shift of reflections,[40,41] but also to the different morphology of the film (regular geometry) compared to that of the compound (strongly irregular morphology). Observing the spectrum of the thermoformed samples, a general confirmation of the peaks obtained on the extruded films can be seen (in this case, the shifts are truly minimal).

However, the presence of the PLA peak at 2θ=16.6° associated with the reflections 200/100 emerges significantly. This result is caused by the increase in crystallinity of the polymeric phases of B-TPS1 following the thermoforming process. As expected, the gradual heating of the extruded film during the thermoforming process results in crystallization of PLA, which is reflected in variations of the XRD spectrum and, in particular, in the emergence of the peak at 2θ=16.6°, not visible in film samples. The result is confirmed by the analysis conducted by Ref. [42], who highlighted the formation of a peak around 16.8°, precisely following an annealing process operated on a PLA-based material.

FTIR Analysis

Spectra of the B-TPS1 compound are summarized in Figs. 6, 7 and 8. In the "functional group zone" (Fig. 6a) the spectrum shows a widened band around 3000 cm^{-1} which is attributable to the stretching vibrations of the hydroxyls groups that characterize TPS. The relative intensity of the band in the B-TPS1 compound is reduced compared to the spectrum of neat TPS, also in relation to the further thermo-mechanical process to which TPS was subjected during reactive extrusion. The absorption band generated by the superposition of the signals given by the stretching vibrations of the —OH bonds appear as a band with many local maximum points. In particular, the band with maximum at 2997 cm^{-1} is attributed to the stretching of the CH_3 groups of PLA, the bands centered at 2958 and 2875 cm^{-1} are both attributed to the stretching vibrations of the CH_2 and CH_3 groups, respectively. present in PBAT. These last two bands partially overlap the absorptions bands at 2947 and 2882 cm^{-1} both related to the stretching vibrations of the CH bonds

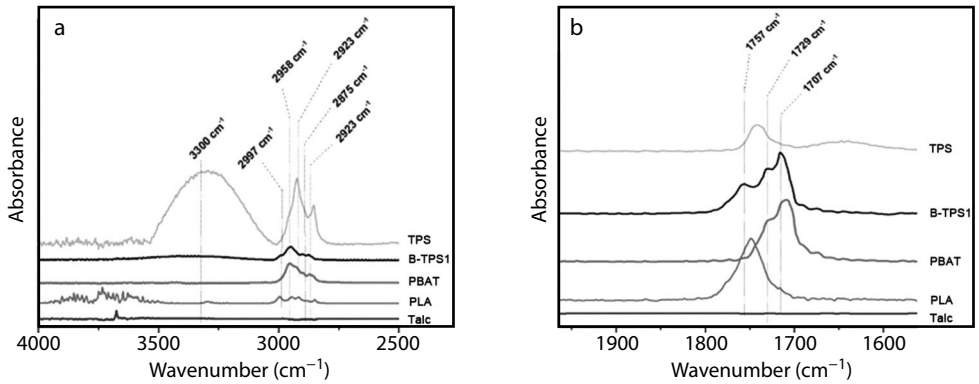

Fig. 6 FTIR spectra of the compound B-TPS1: (a) 4000–2500 cm^{-1} and (b) 1964–1562 cm^{-1}.

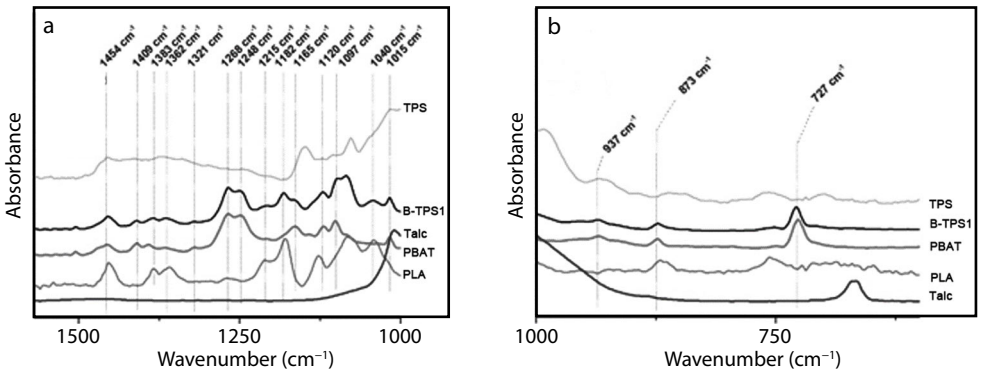

Fig. 7 FTIR spectra of the compound B-TPS1: (a) 1650–1000 cm^{-1} and (b) 1000–600 cm^{-1}.

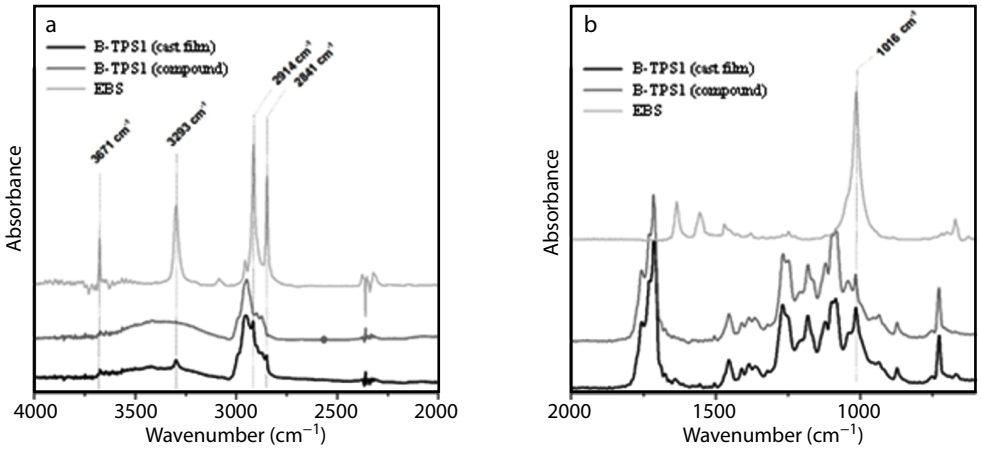

Fig. 8 FTIR spectra of B-TPS1 after extrusion compounding and cast extrusion.

on the PLA molecule. The low intensity band with maximum at 2923 cm^{-1} in the neat TPS spectrum is completely camouflaged in the spectrum of the compound by the presence of more marked absorptions relative to the other components.[43] The presence of the absorptions generated by PLA and PBAT are clearly observed in the spectral zone of the carbonyl groups (Fig. 6b). These two polymers are identifiable within the B-TPS1 compound due to the presence of intense absorption peaks at 1757 cm^{-1} relative to the carbonyl peak of PLA, and of the double band with maxima at 1729 and 1707 cm^{-1} of PBAT. The double carbonyl peak reflects the particular molecular structure of the PBAT copolymer, where one repetitive unit has a carboxylic group conjugated with an aromatic ring and the second unit is made of a carboxylic group in α to an alkyl chain.[36] Considering TPS structure is rich with carboxylic groups, it is interesting to notice the signal indicating its presence is missing (absence of the third carbonyl peak). This absence can be justified by the low starting intensity[37] of the carbonyl signal in the TPS spectrum, centered at 1740 cm^{-1}, as well as by its partial overlap with the absorption peak at 1729 cm^{-1} of PBAT. In the area defined "finger print" (Fig. 8a), the absorptions generated by the presence of PBAT in the compound prevail although the high intensity of some of these signals is attributable to the superposition of homologous

signals in the spectrum of PLA, as it shares the polyester structure of PBAT. PBAT and PLA have, for example, the absorption band at 1454 cm^{-1} in common, attributed in PLA to the bending of the CH_3 groups and in PBAT to the bending in the plane of the CH_2 groups. The band at 1409 cm^{-1} is related to PBAT only and is attributable to the bending of the $O-CH_2$ group. The absorptions at 1383 and 1362 cm^{-1} associated, respectively, to the out-of-plane bending of the CH_2 groups in PLA and to the bending of the CH bond in the methyl groups of PBAT overlap in the spectrum of the B-TPS1 formulation giving rise to a double peak.

The absorption band at 1321 cm^{-1} and the absorptions that generate the double band at 1268 and 1248 cm^{-1} can be attributed to PBAT alone. The absorptions occurring at 1215 and 1182 cm^{-1} are generated by PLA, however, the intensity of these two bands is rather low compared to other signals in the spectrum,[44] due to the low amount of PLA inside the formulation. Nonetheless, the intensity of the band is sufficient to accommodate the shoulder at 1165 cm^{-1}, generated by the of the absorption caused by the stretching of the C—H bonds of PBAT. The same stretching vibrations are equally responsible for absorption at 1097 cm^{-1}. The frequent superposition of the spectra between PLA and PBAT also appears in the medium intensity band at 1120 cm^{-1} which is attributable to the stretching of the CH groups in PBAT and the stretching of the C—O—C bond in PLA. Some PLA bands also coincide with the TPS spectrum profile. In particular, at 1080 cm^{-1} there is an absorption band in the spectrum of the blend which is generated, both in TPS and in PLA, by the vibrations of the C—O—C group, a functional group present on the structure of both components. The absorption at 1040 cm^{-1}, generated by the vibration of the $C-CH_3$ bond, present on the main skeleton of the molecule, is instead attributed to PLA alone.[44] The superposition of the bands locating at 1015 cm^{-1} in the spectra of PBAT and TPS, attributable to the stretching vibrations of the C—O—C group in common between the two molecules, generates three medium intensity bands centered at 1015, 937 and 873 cm^{-1} (Fig. 7b). Lastly, the aromatic ring placed on one of the repetitive units of PBAT is responsible for the out-of-plane bending vibrations of the =C—H bond which appear as a band at 727 cm^{-1} in the spectrum of the B-TPS1 compound. In conclusion, the spectral analysis of the blend B-TPS1 is attributable to signals present in the spectra of the individual components. The appearance of bands or the disappearance of absorptions initially present in the spectra of pure substances was not found. It is therefore possible to testify the absence of reactivity between the components of the B-TPS1 compound.

Furthermore, the FTIR tests carried out on the film sample produced by cast extrusion using the compound B-TPS1 did not show significant changes in the spectrum (Fig. 8), except for minor rearrangements related to the mobility of the amide wax (EBS), whose peaks are more visible after the cast extrusion process of the B-TPS1 formulation.

Scanning Electron Microscopy (SEM)

Fig. 9 shows the cross section of the sample B-TPS1. PBAT and PLA form a co-continuous phase in accordance with Ref. [45]. It is also possible to note the ductile behavior of the PBAT phase. PBAT exhibits plastic deformation, spreading itself over the

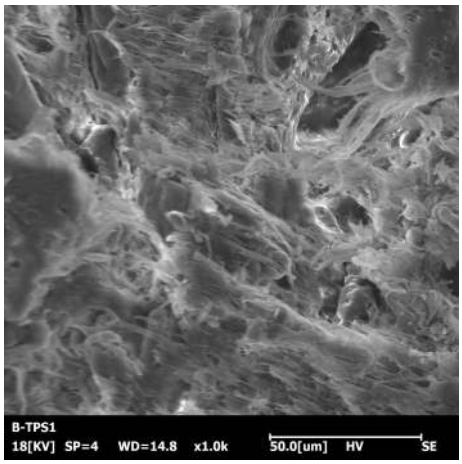

Fig. 9 SEM image of the cross section of the B-TPS1.

cross section of the sample and partially obscuring the visibility of other phases. It is however possible to notice the presence of some large agglomerates (globules) of starch that are not perfectly homogenized in the polyester matrix, not exhibiting an ideal thermoplastic flow in accordance with Refs. [29, 46]. Indeed, the presence of these pellets is very limited in number and size, thus being able to conclude that most of the starch pellets are well dispersed and distributed within the matrix. However, there is no clear division at the interface between the polyesters and the thermoplastic starch as observed in literature,[46] confirming the good homogeneity of the material.

Analysis of the Mechanical Properties of the Extruded Film

Fig. 10 shows the trend of the stress-strain curves for extruded films. The trends show an elastic-plastic behavior of the material both in machine direction and in transversal direction tests. The material exhibits an initial elastic behavior that ends with the yield point, followed by a moderate elongation before exhibiting ductile fracture.[47] Basically, the material exhibits the behavior of a stiff and resistant plastic material (for example, polyamide), with a low elongation at break (>5%), although not as low as in materials with brittle behavior (1%–5%).[48] Difference in properties between samples of B-TPS1 in machine direction and transversal direction are highlighted from the analysis of results in Table 7. In the first case, the elastic modulus E_y is about 360 MPa, 20% higher than the elastic modulus calculated for specimens in transversal direction. This result is attributable to the orientation effect of the polymer chains obtained during cast extrusion. The cast extrusion process promotes an alignment of the chains themselves in the direction of extrusion, similar to what occurs in the filming processes.[49] At the same time, during the extrusion process, the film is slightly stretched in the direction of extrusion (machine direction) due to the action of the pulling unit. This effect can determine a further preferential alignment of the polymer chains in the direction of extrusion, but also favor an increase in the crystallinity of the material and, therefore, increase its elastic modulus and stiffness.[50]

Film samples in machine direction also show a higher yield stress σ_y and fracture stress σ_b, compared to those in transversal direction. Differences in the measured values are testified up to 20%. Elongation at break ε_b values are 13% and 9%

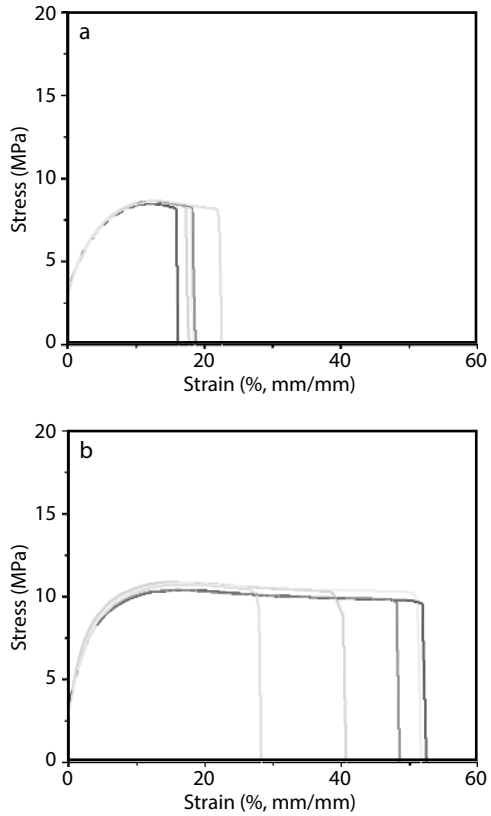

Fig. 10 Stress-strain trends of B-TPS1 film by cast extrusion: (a) transversal direction, (b) machine direction.

Table 7 Data calculated from the analytical elaboration of stress-strain curves reported in Fig. 10.

Sample	E_y (MPa)	σ_y (MPa)	σ_b (MPa)	ε_b (%)
B-TPS1 TD_A	345	8.0	24.6	10.0
B-TPS1 TD_B	251	7.2	21.9	--
B-TPS1 TD_C	305	7.9	24.0	9.7
B-TPS1 TD_D	352	7.5	23.1	6.7
B-TPS1 TD_E	266	7.3	22.7	10.3
Average	303	7.6	23.3	9.2
Sample	E_y (MPa)	σ_y (MPa)	σ_b (MPa)	ε_b (%)
B-TPS1 MD_A	365	9.1	27.8	7.2
B-TPS1 MD_B	272	7.8	23.8	15.4
B-TPS1 MD_C	386	9.8	30.0	10.4
B-TPS1 MD_D	428	10.3	31.5	15.3
B-TPS1 MD_E	352	9.9	30.4	16.6
Average	361	9.4	28	13.0

in machine and transversal direction, respectively. Other than the significant increase in ductility in machine direction, the elongation at break was 5% over the typical threshold of maximum elongation at break of plastic materials characterized brittle behavior. Therefore, this result allows us to confirm that B-TPS1 films can be classified as a stiff and resistant plastic material, which, however, exhibits a ductile fracture.

Figs. 11 and 12 show the fracture behavior, of film samples in machine and transversal direction, confirming, in both cases, a similar ductile fracture behavior typical of stiff and resistant materials.

Permeability

Permeability tests were conducted on 500 μm thick films. The experimental results are summarized in Fig. 13, where a plot of OTR (oxygen transmission rate) versus time is reported. The values calculated considering pure oxygen (100%) as carrier gas and air (21% oxygen) are summarized in Table 8. PBAT has a rather slow crystallization kinetic, this was confirmed by crystallinity data from the analysis of the thermograms and diffractograms of films. The lack of crystalline structures favors the establishment of a large amorphous phase. Therefore, the passage of oxygen molecules is not sufficiently hindered thus causing a rather high oxygen permeability of the material.

This result is in good agreement with that reported in literature.[51,52] The researchers found that the crystallization of PBAT, slower than that of other polyesters such as, for example, PBS did not allow to generate a path as tortuous as the one generated in semi-crystalline PBS, characterized by articulated crystalline structures. This was reflected in a significant increase in the oxygen permeability of PBAT-based materials, analogously to what has been found in the present experiment.

Light Transmission Spectrum

The light transmission spectrum of the film sample in the UV-Vis range is shown in Fig. 14. The material shields the light in the range 190–300 nm, *i.e.*, in the area with the highest energy, while it reaches transmission values of up to 50% (maximum value) for wavelengths corresponding to the near ultraviolet region and in the visible spectrum. This aspect must be strictly taken into account in the use of formulations for the manufacture of containers for packaging of fresh dairy products. For example, several molecules in milk are responsive to light, acting as photosensitizers, including Rb, protoporphyrin, hematoporphyin, chlorophyll a and b, and unidentified tetrapyrroles.[53] The alteration of these molecules can compromise the taste and organoleptic characteristics of the fresh product. Furthermore, the wavelengths at which these modifications are more invasive, altering the taste of milk, are those higher than 250 nm and, in particular, those around 500 nm,[54] where the material B-TPS1 is not very effective in shielding the light radiation.

The poor protection capacity of the formulation against the transmission of light radiations, especially in the near ultraviolet and, even more so, in the visible spectrum, is certainly to be linked to the low crystallinity of PBAT,[55] but also to the low content of mineral fillers (*i.e.*, talc in this formulation).[56] Although the kind of talc used in the present formulation has a micronized and lamellar configuration, talc is notoriously not very effective at shielding light radiations, which is why, plastic materials are commonly additivated with titanium dioxide.

Indeed, titanium dioxide is much more effective at shielding light radiation, even and especially when it is present in modest quantities within the formulation as demonstrated in literature.[53]

Chemical Inertia

Fig. 15 summarizes the results of the chemical inertness tests performed on B-TPS1 extruded film samples. NaOH and HCl solutions simulate contact with foods and beverages of a basic or acidic nature, respectively, as well as simulating (in the case of NaOH) the alkaline environment generated by soaps. The 3% NaCl solution simulated the attack of chlorides in the presence

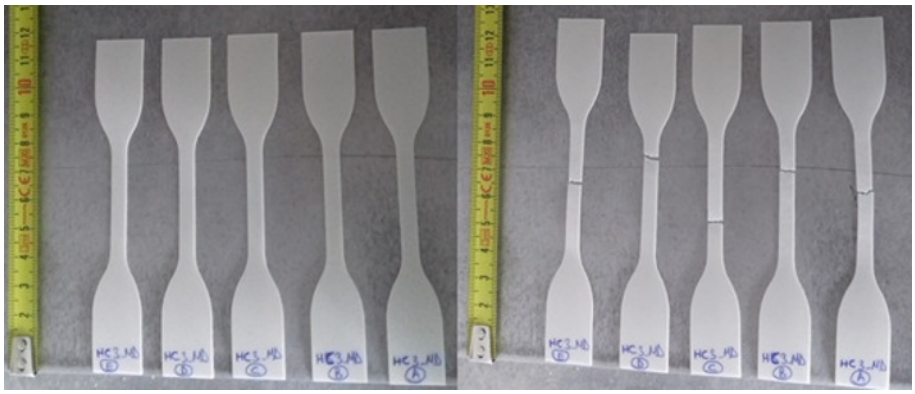

Fig. 11 B-TPS1 film samples in machine direction before and after fracture.

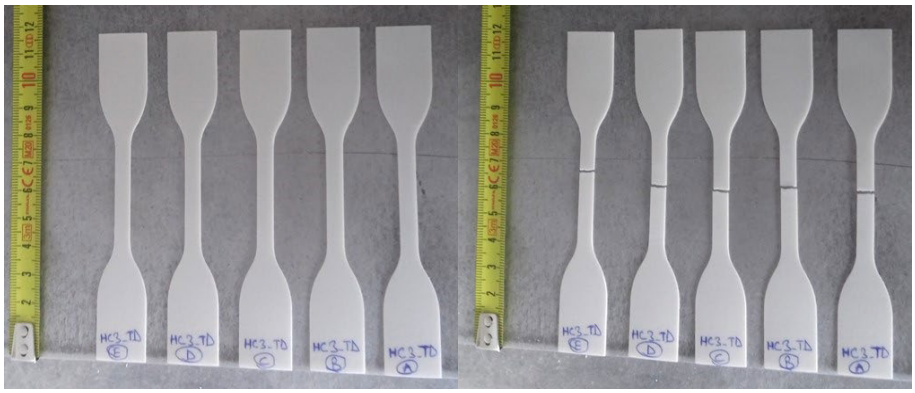

Fig. 12 B-TPS1 film samples in transversal direction before and after fracture.

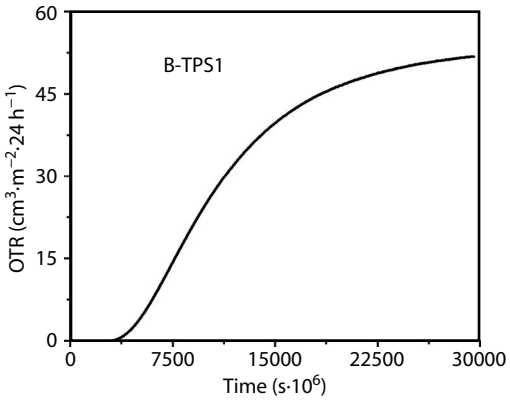

Fig. 13 Permeability evaluated on 500 μm-thick films and normalized on 100% oxygen content.

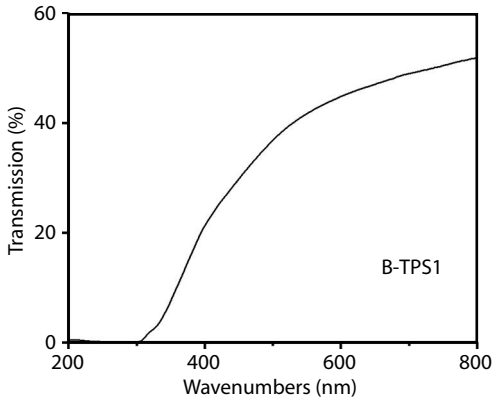

Fig. 14 UV-Vis spectrum on B-TPS1 film.

Table 8 Permeability of B-TPS1 films.

Sample	OTR 21% ($cm^3 \cdot m^{-2} \cdot 24h^{-1}$)	OTR 100% ($cm^3 \cdot m^{-2} \cdot 24h^{-1}$)
B-TPS1	10.81	51.49

of salty foods. Ethanol, vinegar and seed oil are, on the other hand, which are normally used in food preparations, turn out to be commonly the most aggressive components for plastic products. In particular, oil is able to solubilize some polymers or, in milder cases, to impregnate them by means of soaking mechanisms.[57]

Vinegar creates an acidic environment causing a high risk in presence of materials based on polyester resins. Indeed, in the case of biodegradable polyesters, contact with vinegar can catalyze the hydrolysis of the material itself, favoring degradation mechanisms of the plastic material and, at the same time, causing potential migration of substances with a lower molecular weight to the food. Ethanol, an organic solvent with high polarity, can, like oil, solubilize polyesters by soaking mechanism.

B-TPS1 films are sensitive to aqueous solutions. This is attributed to the presence of TPS in the formulation, which, in the form of native starch, is extremely hydrophilic and water-soluble.[58] For this reason, the dispersion and distribution of TPS in the polyesters during the compounding phase appears fundamental. In this work, this was possible by the use

https://doi.org/10.1007/s10118-022-2734-0

Fig. 15 Chemical inertia carried out on B-TPS1 films by cast extrusion.

of sufficiently high shear forces, together with high temperatures typical of the co-rotating twin screw extrusion process, in accordance with Ref. [59]. The films are also sensitive to a basic environment where, in addition to the water solubilization effect on TPS, there is also a phenomenon of hydrolysis catalyzed by the alkaline environment on the polyesters present in the formulation in accordance with Ref. [60].

Lastly, the film shows a clear color change of the surface in tests carried out in the presence of vinegar. This result is caused by the absorption of pigments present in vinegar (chlorophyll, quercetin, leukoanthocyanins and catechins), which are adsorbed selectively and by affinity on the surface of the film, even in the absence of acid attack, due to their more hydrophobic character compared to other components inside vinegar.[61]

Thermal Resistance

The thermal resistance test was carried out by placing the thermoformed product directly in contact with hot water, where instant contact is the determining factor. A progressive heating of the liquid inside the container (as well as water heating to test microwave heating resistance) would not be as significative because polyesters would not be affected by a gradual heating, since they have the ability to recrystallize rather quickly due to the effect of thermal annealing.[62] Conversely, they are not, in general, able to effectively counteract the thermal shock that is generated by direct and immediate contact with large quantities of hot liquid, as is the case of the present test.

The thermoformed product made with the B-TPS1 formulation passed both tests at 65 and 100 °C, exhibiting full geometric correspondence at the end of contact with hot water (Fig. 16), except for negligible shrinkage. Such a performing behavior of the B-TPS1 formulation was not expected, since the main polymeric phases are PBAT and TPS, respectively 45% and 25%, and PLA constitutes a third phase at 20%. All constituents have T_g, VICAT and HDT definitely lower than 100 °C. The unexpected positive behavior of the blend is presumably attributable to the substantial immiscibility and poor interfacial affinity between the three polymeric phases present in the formulation, which alter the creep dynamics even at high temperatures.

The equations [*Wu, S. Polymer Interface and Adhesion (Marcel Dekker, New York, 1982)*] those have been used for calculating the surface and interfacial tensions reported in Tables 9 and 10 are as follows:

$$\gamma_{12} = \gamma_1 + \gamma_2 - 2\left(\sqrt{\gamma_1^d \gamma_2^d} + \sqrt{\gamma_1^p \gamma_2^p}\right) \quad (4)$$

Fig. 16 Thermoformed items with B-TPS1 compound: as-is (left); after being tested at 65 °C (middle); after being tested at 100 °C (right).

$$\gamma_{12} = \gamma_1 + \gamma_2 - \frac{4\gamma_1^d\gamma_2^d}{\gamma_1^d + \gamma_2^d} - \frac{4\gamma_1^p\gamma_2^p}{\gamma_1^p + \gamma_2^p} \quad (5)$$

PLA and PBAT have rather similar surface tension values, also with regards to their dispersive and polar components (Tables 9 and 10). Nonetheless, their interfacial tension stays relatively low, either it is calculated with the equation (Eq. 4) considering the geometric mean proposed in Ref. [63] or with the equation (Eq. 5) considering the harmonic mean proposed in Ref. [64].

Basically, PLA and PBAT are immiscible in almost all proportions, but still substantially similar. In contrast, TPS exhibits very different surface tension values compared to PLA and PBAT, in particular, the dispersive component which is much lower. Consequently, the interfacial tensions of TPS with polyesters are much higher (one order of magnitude greater), which is an evident sign of very low affinity. In agreement with literature,[65] the difference in the polarity between hydrophilic starch and hydrophobic PBAT and PLA generates a high interfacial tension between TPS and the polyesters. PLA and PBAT are expected to form a co-continuous phase when blended in the ratio 45:20 as in B-TPS1 (Fig. 10). Instead, starch pellets are expected to distribute in the polymeric matrix in agreement with literature,[63] which confirms the substantial incompatibility of starch with PBAT/PLA. This is also expected to cause an increase in Young's modulus (stiffness) of the blend in agreement with literature.[65] Therefore, high chemical incompatibility and high immiscibility of the polymeric phases (PLA and PBAT on one hand and TPS on the other hand) causes them to repel each other at molecular level, hindering the reciprocal sliding of the chains due to low interfacial affinity, thus decreasing the mutual capacity to slide and, therefore, limiting deformation of the softened material.

Indeed, the high thermal resistance of B-TPS1 thermoformed products can be justified, in this case, only thanks to the melting temperature values of the three polymers in B-TPS formulation, which are much higher than 100 °C. This result is therefore of extreme practical interest, as it demonstrates how it is possible to add a bioavailable polymer such as starch (albeit plasticized) to a blend of common compostable polyesters (such as PLA and PBAT), without compromising performance in terms of thermal resistance of the compound and of items manufactured with it, in fact improving them and providing a product suitable for contact with hot food.

Resistance to Compression Load of Thermoformed Products

Fig. 17 shows the compressive behavior of the thermoformed products. Fig. 18, on the other hand, shows precisely how the test is performed, it involves the use of a large compression plate to homogeneously deform the product along the entire surface. Table 11 shows the analytical results obtained from the compression test on the thermoformed products. The obtained trends are very similar to the expected theoretical trend described previously in Fig. 2. As previously mentioned, adjacent peaks along the force versus displacement curve are to be ascribed to the sequential failure of the ribs which endow the thermoformed products affecting the deformation behavior of samples. B-TPS1 is confirmed as a stiff and resistant plastic material. The thermoformed products show a flexible behavior consistent with the tensile test, a low stiffness, a modest overall resistance to compression and a high sensitivity to crosshead speed variations *(i.e.*, of the deformation rate). After all, PBAT has a high flexibility and a modest resistance. Mechanical characteristics of PBAT, being the main polymeric phase, are

Table 9 Surface tension of biopolymers and interfacial tensions of TPS.

Sample	γ (mJ/m^2)	γ_d (mJ/m^2)	γ_p (mJ/m^2)	$\gamma_{TPS/Polymer}$[61] (mJ/m^2)	$\gamma_{TPS/Polymer}$[62] (mJ/m^2)
PLA	50	37	13	2.61	5.11
PBAT	53	42	11	4.06	7.85
TPS	32	20	12	0.00	0.00

Table 10 Surface tension of biopolymers and interfacial tensions of PLA.

Sample	γ (mJ/m^2)	γ_d (mJ/m^2)	γ_p (mJ/m^2)	$\gamma_{PLA/Polymer}$[61] (mJ/m^2)	$\gamma_{PLA/Polymer}$[62] (mJ/m^2)
PLA	50	37	13	0,00	0,00
PBAT	53	42	11	0,24	0,48
TPS	32	20	12	2,61	5,11

https://doi.org/10.1007/s10118-022-2734-0

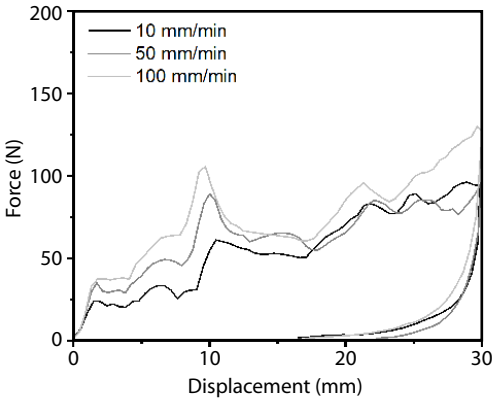

Fig. 17 Compression tests on thermoformed items.

Fig. 18 Compression tests performed on the thermoformed items.

Table 11 Compression test on B-TPS1 thermoformed items: analytical data.

Strain rate (mm/min)	Stiffness (N/mm)	Max load (N)	Strain at max load (mm)	Ultimate Load (N)	Strain at ultimate load (mm)	Elastic recovery (mm)	Strain energy (J)
10	30124	97.18	30.00	97.05	28.9	12.3	2.1
50	42653	98.84	30.02	97.42	29.98	7.65	1.73
100	45165	135.56	30.06	134.67	30.03	12.6	1.6

therefore transferred to the respective thermoformed product, which behaves consistently with the macroscopic characteristics observed in the base polymer which the compound is based on.

Compostability

Compostability tests have been developed recording both the morphological change of the extruded films as shown in Fig. 19, and the mass variation of samples as reported in Table 12. The

Fig. 19 Morphology of the samples after 9 weeks.

Table 12 Trends of mass loss during compostability tests on B-TPS1.

Samples	B-TPS1 (g)
Start	20800
After 1 week	20353
After 2 weeks	19488
After 3 weeks	19227
After 4 weeks	18297
After 5 weeks	17693
After 6 weeks	17647
After 7 weeks	14786
After 8 weeks	14669
After 9 weeks	13708

protocol used for carrying out the compostability tests in ambient conditions is not regulated by a precise normative framework, therefore it is assumed that the validity of the test carried out in this work can be taken into consideration, strictly speaking, only on a comparative basis. From the observation of the experimental results, it emerges that the B-TPS1 material undergoes a progressive weight loss over time, a strong color change that occurs after the first week and intensifies in the following weeks and, finally and a progressive fragmentation of the samples, which decidedly increases starting from week 4.

Sample B-TPS1 was characterized by a rapid weight loss starting from week 7. Based on the observation of the morphology of the samples, it also emerges that the material exhibits a rapid disintegration in ambient conditions. The high rate of mass loss of the B-TPS1 formulation may be, in some way, related to the low crystallinity of PBAT, which is known to affect the degradation phenomena in the composter.[66] Indeed, amorphous materials tend to biodegrade more easily, losing weight very quickly compared to materials with a higher crystallinity degree. Furthermore, the role of crystallinity in the biodegradation capacity of polyesters has been widely studied for PLA-based materials, where the degree of crystallinity itself and the average size of the crystallites are known to strongly influence the biodegradation rate under controlled composting conditions, as reported in literature.[67] Moreover, it has been demonstrated that not only the degree of crystallinity, but also the type of crystalline structure can significantly influence the biodegradation rate of polyesters.[68]

CONCLUSIONS

This sork explores the possibility of using TPS, a bioavailable polymer with a very low environmental footprint, inside a blend with compostable polyesters for the manufacture of rigid and semi-rigid packaging items suitable for the storage of hot foods. The case study concerned, in particular, the use of TPS at 25

https://doi.org/10.1007/s10118-022-2734-0

wt% within a PBAT/PLA (9/4) blend. Reactive extrusion process by means of a co-rotating twin-screw system highlighted the difficult processability of the formulation due to the presence of TPS, which was homogenized within the polyesters only by using high screw speed and, therefore, high shear stresses. Scanning electron microscopy shows the good dispersion of TPS, although the immiscibility of some starch pellets in the PBAT/PLA co-continuous matrix was highlighted. The FTIR spectra do not show, among other things, significant reactive processes in compounding, with the spectrum of the B-TPS1 compound being the sum of the spectra of the individual constituents.

Cast extruded films and thermoformed items display much higher crystallinity degrees of the polymeric phases than those achieved in the compound, a clear sign that reprocessing favors an increase in the crystallinity of the formulation. The thermoformed products have a high heat resistance, probably due to the low affinity between TPS and polyesters which hinders the sliding of the polymeric chains at high temperatures, increasing the effective thermal resistance (100 °C) in contact with hot liquids. Furthermore, the mechanical tests reveal an elastoplastic behavior with good stiffness but modest ductility/toughness, comparable to stiff and resistant plastic materials. Finally, the B-TPS1 formulation quickly loses mass in composting tests in ambient conditions, disintegrating effectively and demonstrating an excellent compromise between thermal resistance at high temperatures and biodegradation rate. This makes the formulation particularly suitable for the production of packaging for hot food.

In this regard, it is noted that B-TPS1 exhibits a modest protection both to the transmission of gaseous species (oxygen) and to the transmission of light radiations. This aspect must be strictly taken into consideration in relation to the possible practical applications of the formulation.

NOTES

The authors declare no competing financial interest.

REFERENCES

1 Patel, M., Do Biopolymers Fulfill Our Expectations Concerning Environmental Benefits? in: Chiellini, E., Solaro, R. (Eds.), *Biodegradable Polymers and Plastics*. Springer US, Boston, MA, **2003**, pp. 83–102.

2 Desole, M. P.; Aversa, C.; Barletta, M.; Gisario, A.; Vosooghnia, A. Life cycle assessment (LCA) of PET and PLA bottles for the packaging of fresh pasteurised milk: the role of the manufacturing process and the disposal scenario. *Packaging Technol. Sci.* **2021**, *35*, 135–152.

3 Cappiello, G.; Aversa, C.; Genovesi, A.; Barletta, M. Life cycle assessment (LCA) of bio-based packaging solutions for extended shelf-life (ESL) milk. *Environ. Sci. Pollut. Res. Int.* **2022**, *29*, 18617–18628.

4 Broeren, M. L. M.; Kuling, L.; Worrell, E.; Shen, L. Environmental impact assessment of six starch plastics focusing on wastewater-derived starch and additives. *Resources, Conservation and Recycling* **2017**, *127*, 246–255.

5 Bangar, S. P.; Whiteside, W. S.; Ashogbon, A. O.; Kumar, M. Recent advances in thermoplastic starches for food packaging: a review. *Food Packaging and Shelf Life* **2021**, *30*, 100743.

6 Pan, H.; Ju, D.; Zhao, Y.; Wang, Z.; Yang, H.; Zhang, H.; Dong, L. Mechanical properties, hydrophobic properties and thermal stability of the biodegradable poly(butylene adipate-*co*-terephthalate)/maleated thermoplastic starch blown films. *Fibers Polym.* **2016**, *17*, 1540–1549.

7 Fourati, Y.; Tarrés, Q.; Mutjé, P.; Boufi, S. PBAT/thermoplastic starch blends: effect of compatibilizers on the rheological, mechanical and morphological properties. *Carbohydr. Polym.* **2018**, *199*, 51–57.

8 Garalde, R.A.; Thipmanee, R.; Jariyasakoolroj, P.; Sane, A. The effects of blend ratio and storage time on thermoplastic starch/poly(butylene adipate-*co*-terephthalate) films. *Heliyon* **2019**, *5*, e01251.

9 Lekube, B.M.; Fahrngruber, B.; Kozich, M.; Wastyn, M.; Burgstaller, C. Influence of processing on the mechanical properties and morphology of starch-based blends for film applications. *J. Appl. Polym. Sci.* **2019**, *136*, 47990.

10 Dammak, M.; Fourati, Y.; Tarrés, Q.; Delgado-Aguilar, M.; Mutjé, P.; Boufi, S. Blends of PBAT with plasticized starch for packaging applications: Mechanical properties, rheological behaviour and biodegradability. *Indust. Crops Prod.* **2020**, *144*, 112061.

11 Liu, W.; Wang, Z.; Liu, J.; Dai, B.; Hu, S.; Hong, R.; Xie, H.; Li, Z.; Chen, Y.; Zeng, G. Preparation, reinforcement and properties of thermoplastic starch film by film blowing. *Food Hydrocolloids* **2020**, *108*, 106006.

12 Pokhrel, S.; Sigdel, A.; Lach, R.; Slouf, M.; Sirc, J.; Katiyar, V.; Bhattarai, D. R.; Adhikari, R. Starch-based biodegradable film with poly(butylene adipate-*co*-terephthalate): preparation, morphology, thermal and biodegradation properties. *J. Macromol. Sci.* **2021**, *Part A 0*, 610–621.

13 Diyana, Z. N.; Jumaidin, R.; Selamat, M. Z.; Ghazali, I.; Julmohammad, N.; Huda, N.; Ilyas, R. A. Physical properties of thermoplastic starch derived from natural resources and its blends: a review. *Polymers* **2021**, *13*, 1396.

14 Khan, B.; Bilal Khan Niazi, M.; Samin, G.; Jahan, Z. Thermoplastic starch: a possible biodegradable food packaging material—a review. *J. Food Proc. Eng.* **2017**, *40*, e12447.

15 Aldas, M.; Pavon, C.; López-Martínez, J.; Arrieta, M. P. Pine resin derivatives as sustainable additives to improve the mechanical and thermal properties of injected moulded thermoplastic starch. *Appl. Sci.* **2020**, *10*, 2561.

16 Pavon, C.; Aldas, M.; López-Martínez, J.; Hernández-Fernández, J.; Arrieta, M. P. Films based on thermoplastic starch blended with pine resin derivatives for food packaging. *Foods* **2021**, *10*, 1171.

17 Quiles-Carrillo, L.; Montanes, N.; Pineiro, F.; Jorda-Vilaplana, A.; Torres-Giner, S. Ductility and toughness improvement of injection-molded compostable pieces of polylactide by melt blending with poly(ε-caprolactone) and thermoplastic starch. *Materials* **2018**, *11*, 2138.

18 Chapleau, N.; Huneault, M. A.; Li, H. Biaxial orientation of polylactide/thermoplastic starch blends. *Int. Polym. Proc.* **2007**, *22*, 402–409.

19 Suwanmanee, U.; Varabuntoonvit, V.; Chaiwutthinan, P.; Tajan, M.; Mungcharoen, T.; Leejarkpai, T. Life cycle assessment of single use thermoform boxes made from polystyrene (PS), polylactic acid, (PLA), and PLA/starch: cradle to consumer gate. *Int. J. Life Cycle Assess.* **2013**, *18*, 401–417.

20 Zhao, X.; Cornish, K.; Vodovotz, Y. Narrowing the gap for bioplastic use in food packaging: an update. *Environ. Sci. Technol.* **2020**, *54*, 4712–4732.

21 Robertson, G.L. 3 - Packaging and Food and Beverage Shelf Life, in: Subramaniam, P. (Ed.), in *The Stability and Shelf Life of Food (Second Edition)*, Woodhead Publishing Series in Food Science, Technology and Nutrition. Woodhead Publishing, **2016**, pp.

77–106.
22 Panseri, S.; Martino, P. A.; Cagnardi, P.; Celano, G.; Tedesco, D.; Castrica, M.; Balzaretti, C.; Chiesa, L. M. Feasibility of biodegradable based packaging used for red meat storage during shelf-life: a pilot study. *Food Chem.* **2018**, *249*, 22–29.
23 Gerometta, M.; Rocca-Smith, J. R.; Domenek, S.; Karbowiak, T. Physical and chemical stability of PLA in food packaging, in: *Reference Module in Food Science*. Elsevier, **2019**.
24 Larsson, M.; Markbo, O.; Jannasch, P. Melt processability and thermomechanical properties of blends based on polyhydroxyalkanoates and poly(butylene adipate-*co*-terephthalate). *RSC Adv.* **2016**, *6*, 44354–44363.
25 Höhne, C.; Schmidt, R.; Berner, V.; Metzsch-Zilligen, E.; Westphal, E.; Pfaendner, R.; Mack, C. Intrinsic flame retardancy of poly(lactic acid) bead foams. *J. Appl. Polym. Sci.* **2021**, *138*, 50856.
26 Barrena, R.; Font, X.; Gabarrell, X.; Sánchez, A. Home composting versus industrial composting: influence of composting system on compost quality with focus on compost stability. *Waste Manag.* **2014**, *34*, 1109–1116.
27 Kaseem, M.; Hamad, K.; Deri, F. Thermoplastic starch blends: a review of recent works. *Polym. Sci. Ser.* **2012**, *A54*, 165–176.
28 Zhang, Y.; Rempel, C.; Liu, Q. Thermoplastic starch processing and characteristics—a review. *Critic. Rev. Food Sci. Nutrit.* **2014**, *54*, 1353–1370.
29 Phattarateera, S.; Junsook, N.; Kumsang, P.; Aontee, A.; Kerddonfag, N. The ternary blends of TPS/PBAT/PLA films: a study on the morphological and mechanical properties. *Key Eng. Mater.* **2020**, *861*, 170–175.
30 Li, Y.; Zhao, L.; Han, C.; Yu, Y. Biodegradable blends of poly(butylene adipate-*co*-terephthalate) and stereocomplex polylactide with enhanced rheological, mechanical properties and thermal resistance. *Colloid Polym. Sci.* **2020**, *298*, 463–475.
31 Muthuraj, R.; Misra, M.; Mohanty, A. K. Binary blends of poly(butylene adipate-*co*-terephthalate) and poly(butylene succinate): a new matrix for biocomposites applications. *AIP Conference Proceedings* **2015**, *1664*, 150009.
32 Hsieh, Y. T.; Nozaki, S.; Kido, M.; Kamitani, K.; Kojio, K.; Takahara, A. Crystal polymorphism of polylactide and its composites by X-ray diffraction study. *Polymer* **2020**, *J52*, 755–763.
33 Jalali, A.; Huneault, M.A.; Elkoun, S. Effect of thermal history on nucleation and crystallization of poly(lactic acid). *J. Mater. Sci.* **2016**, *51*, 7768–7779.
34 Suryanegara, L.; Nakagaito, A. N.; Yano, H. The effect of crystallization of PLA on the thermal and mechanical properties of microfibrillated cellulose-reinforced PLA composites. *Compos. Sci. Technol.* **2009**, *69*, 1187–1192.
35 Savadekar, N. R.; Kadam, P. G.; Mhaske, S. T. Studies on the effect of nano-alumina on the performance properties of poly(butylene adipate-*co*-terephthalate) composite films. *J. Thermoplastic Compos. Mater.* **2015**, *28*, 1522–1536.
36 Li, X.; Tan, D.; Xie, L.; Sun, H.; Sun, S.; Zhong, G.; Ren, P. Effect of surface property of halloysite on the crystallization behavior of PBAT. *Appl. Clay Sci.* **2018**, *157*, 218–226.
37 Mahieu, A.; Terrié, C.; Agoulon, A.; Leblanc, N.; Youssef, B. Thermoplastic starch and poly(ε-caprolactone) blends: morphology and mechanical properties as a function of relative humidity. *J. Polym. Res.* **2013**, *20*, 229.
38 Castillo, L. A.; López, O. V.; García, M. A.; Barbosa, S. E.; Villar, M. A. Crystalline morphology of thermoplastic starch/talc nanocomposites induced by thermal processing. *Heliyon* **2019**, *5*, e01877.
39 Yu, W.; Wang, X.; Ferraris, E.; Zhang, J. Melt crystallization of PLA/Talc in fused filament fabrication. *Mater. Design* **2019**, *182*, 108013.
40 Aglietti, E. F. The effect of dry grinding on the structure of talc. *Appl. Clay Sci.* **1994**, *9*, 139–147.
41 Holland, H. J.; Murtagh, M. J. An XRD morphology index for talcs: the effect of particle size and morphology on the specific surface area 8. in *Advances in X-ray Analysis*, Springer, **2000**.
42 Gómez-Pachón, E. Y.; Vera-Graziano, R.; Campos, R. M. Structure of poly(lactic-acid) PLA nanofibers scaffolds prepared by electrospinning. *IOP Conf. Ser.: Mater. Sci. Eng.* **2014**, *59*, 012003.
43 Zhai, X.; Wang, W.; Zhang, H.; Dai, Y.; Dong, H.; Hou, H. Effects of high starch content on the physicochemical properties of starch/PBAT nanocomposite films prepared by extrusion blowing. *Carbohydr. Polym.* **2020**, *239*, 116231.
44 Palai, B.; Biswal, M.; Mohanty, S.; Nayak, S. K. *In situ* reactive compatibilization of polylactic acid (PLA) and thermoplastic starch (TPS) blends; synthesis and evaluation of extrusion blown films thereof. *Indust. Crops Products* **2019**, *141*, 111748.
45 Chen, J.; Rong, C.; Lin, T.; Chen, Y.; Wu, J.; You, J.; Wang, H.; Li, Y. Stable co-continuous pla/pbat blends compatibilized by interfacial stereocomplex crystallites: toward full biodegradable polymer blends with simultaneously enhanced mechanical properties and crystallization rates. *Macromolecules* **2021**, *54*, 2852–2861.
46 Ren, J.; Fu, H.; Ren, T.; Yuan, W. Preparation, characterization and properties of binary and ternary blends with thermoplastic starch, poly(lactic acid) and poly(butylene adipate-*co*-terephthalate). *Carbohydr. Polym.* **2009**, *77*, 576–582.
47 Rostiashvili, V. G., Vilgis, T. A. Statistical thermodynamics of polymeric networks, in: Kobayashi, S., Müllen, K. (Eds.), *Encyclopedia of Polymeric Nanomaterials*. Springer Berlin Heidelberg, Berlin, Heidelberg, **2014**, pp. 1–18.
48 Roberts, D. R. T., Holder, S. J. Mechanochromic systems for the detection of stress, strain and deformation in polymeric materials. *J. Mater. Chem.* **2011**, *21*, 8256–8268.
49 Li, X.; Ai, X.; Pan, H.; Yang, J.; Gao, G.; Zhang, H.; Yang, H.; Dong, L. The morphological, mechanical, rheological, and thermal properties of PLA/PBAT blown films with chain extender. *Polym. Adv. Technol.* **2018**, *29*, 1706–1717.
50 Zhang, T.; Han, W.; Zhang, C.; Weng, Y. Effect of chain extender and light stabilizer on the weathering resistance of PBAT/PLA blend films prepared by extrusion blowing. *Polym. Degrad. Stabil.* **2021**, *183*, 109455.
51 de Matos Costa, A. R.; Crocitti, A.; Hecker de Carvalho, L. H.; de Carroccio, S. C.; Cerruti, P.; Santagata, G. Properties of biodegradable films based on poly(butylene succinate) (PBS) and poly(butylene adipate-*co*-terephthalate) (PBAT) blends. *Polymers* **2020**, *12*, 2317.
52 Bumbudsanpharoke, N.; Wongphan, P.; Promhuad, K.; Leelaphiwat, P.; Harnkarnsujarit, N. Morphology and permeability of bio-based poly(butylene adipate-*co*-terephthalate) (PBAT), poly(butylene succinate) (PBS) and linear low-density polyethylene (LLDPE) blend films control shelf-life of packaged bread. *Food Control* **2022**, *132*, 108541.
53 Johnson, D. S.; Duncan, S. E.; Bianchi, L. M.; Chang, H. H.; Eigel, W. N.; O'Keefe, S. F. Packaging modifications for protecting flavor of extended-shelf-life milk from light. *J. Dairy Sci.* **2015**, *98*, 2205–2214.
54 Cladman, W.; Scheffer, S.; Goodrich, N.; Griffiths, M. W. Shelf-life of milk packaged in plastic containers with and without treatment to reduce light transmission. *Int. Dairy J.* **1998**, *8*, 629–636.
55 Xiao, T.; Wang, J.; Yang, S.; Zhu, Y.; Li, D.; Wang, Z.; Feng, S.; Bu, L.; Zhan, X.; Lu, G. Film-depth-dependent crystallinity for light transmission and charge transport in semitransparent organic solar cells. *J. Mater. Chem. A* **2020**, *8*, 401–411.
56 Jain, S.; Reddy, M. M.; Mohanty, A. K.; Misra, M.; Ghosh, A. K. A new biodegradable flexible composite sheet from poly(lactic acid)/poly(ε-caprolactone) blends and micro-talc. *Macromol.*

Mater. Eng. **2010**, *295*, 750–762.
57 Aboul-Gheit, A. K.; Khalil, F. H.; Abdel-Moghny, T. Adsorption of spilled oil from seawater by waste plastic. *Oil Gas Sci. Technol. - Rev. IFP* **2006**, *61*, 259–268.
58 Mitrus, M.; Combrzyński, M.; Kupryaniuk, K.; Wójtowicz, A.; Oniszczuk, T.; Kręcisz, M.; Matysiak, A.; Smurzyńska, A.; Mościcki, L. A study of the solubility of biodegradable foams of thermoplastic starch. *J. Ecol. Eng.* **2016**, (17), 184–189.
59 Yu, J.; Wang, N.; Ma, X. The effects of citric acid on the properties of thermoplastic starch plasticized by glycerol. *Starch* **2005**, *57*, 494–504.
60 Tham, C. Y.; Hamid, Z. A. A.; Ahmad, Z.; Hanafi, I. Surface modification of poly(lactic acid) (PLA) *via* alkaline hydrolysis degradation. *Adv. Mater. Res.* **2014**, *970*, 324–327.
61 Makhdoumi, P.; Naghshbandi, M.; Ghaderzadeh, K.; Mirzabeigi, M.; Yazdanbakhsh, A.; Hossini, H. Micro-plastic occurrence in bottled vinegar: qualification, quantification and human risk exposure. *Proc. Safety Environ. Prot.* **2021**, *152*, 404–413.
62 Chiu, H. T.; Huang, S. Y.; Chen, Y. F.; Kuo, M. T.; Chiang, T. Y.; Chang, C. Y.; Wang, Y. H. Heat treatment effects on the mechanical properties and morphologies of poly(lactic acid)/poly(butylene adipate-co-terephthalate) blends. *Int. J. Polym. Sci.* **2013**, e951696.
63 Nofar, M.; Maani, A.; Sojoudi, H.; Heuzey, M. C.; Carreau, P. J. Interfacial and rheological properties of PLA/PBAT and PLA/PBSA blends and their morphological stability under shear flow. *J. Rheol.* **2015**, *59*, 317–333.
64 Huneault, M.A.; Li, H. Preparation and properties of extruded thermoplastic starch/polymer blends. *J. Appl. Polym. Sci.* **2012**, *126*, E96–E108.
65 Shirai, M. A.; Olivato, J. B.; Garcia, P. S.; Müller, C. M. O.; Grossmann, M. V. E.; Yamashita, F. Thermoplastic starch/polyester films: effects of extrusion process and poly(lactic acid) addition. *Mater. Sci. Eng.* **2013**, *C33*, 4112–4117.
66 Cai, H.; Dave, V.; Gross, R. A.; McCarthy, S. P. Effects of physical aging, crystallinity, and orientation on the enzymatic degradation of poly(lactic acid). *J. Polym. Sci., Part B: Polym. Phys.* **1996**, *34*, 2701–2708.
67 Pantani, R.; Sorrentino, A. Influence of crystallinity on the biodegradation rate of injection-moulded poly(lactic acid) samples in controlled composting conditions. *Polym. Degrad. Stabil.* **2013**, *98*, 1089–1096.
68 Cho, K.; Lee, J.; Kwon, K. Hydrolytic degradation behavior of poly(butylene succinate)s with different crystalline morphologies. *J. Appl. Polym. Sci.* **2001**, *79*, 1025–1033.